Journal of Inflammation Research

Dovepress
Taylor & Francis Group

Open Access Full Text Article

ORIGINAL RESEARCH

Exploring the Anti-Inflammatory and Anti-NET Properties of Zidian Zhenxiao Granule in IgA Vasculitis: A Network Pharmacology and Proteomic Study

Xiaofang Zhang[1], Minghang Yang[1], Xiaozheng Duan[1], Xiaochun Feng[1,*], Yanqiu Fang[1,2,*]

[1]School of Chinese Medicine, Changchun University of Chinese Medicine, Changchun, People's Republic of China; [2]Center of Reproductive Medicine, Jilin Province People's Hospital, Changchun, People's Republic of China

*These authors contributed equally to this work

Correspondence: Xiaochun Feng; Yanqiu Fang, School of Chinese Medicine, Changchun University of Chinese Medicine, 1035 Boshuo Road, Changchun, 130117, People's Republic of China, Email 18852099003@163.com; yq.fang0920@163.com

Background and Purpose: Immunoglobulin A vasculitis (IgAV) is the most common systemic vasculitis of childhood. Zidian Zhenxiao granule (ZDZX), a 9-herb formula optimized through decades of clinical practice, uniquely integrates anti-inflammatory and immunomodulatory properties. However, its mechanisms targeting neutrophil extracellular traps (NETs) and thromboinflammatory pathways in combating IgAV remain unclear. This study aimed to investigate the main component of ZDZX and its underlying mechanism in IgAV treatment.

Methods: Combining UHPLC-QE-MS/MS, network pharmacology, 4D-FastDIA proteomics, and a gliadin-induced IgAV murine model, we systematically deciphered ZDZX's renoprotective and anti-inflammatory mechanisms.

Results: 19 key components were identified in ZDZX, targeting 46 IgAV-associated proteins, predominantly enriched in TNF and IL-17 signaling pathways. In vivo, ZDZX significantly reduced levels of blood urea nitrogen (BUN) and creatinine (p <0.01), attenuated renal IgA/C3 deposition, and improved hematological parameters. Proteomics revealed 27 differentially expressed proteins (DEPs) (FDR <0.05), including MPO, IL-17, MMP2, C3 and COL1A1, implicating coagulation cascades and neutrophil extracellular trap (NET) formation. Additionally, ZDZX downregulated renal IL-6, TNF-α, and citrullinated histone H3 (CitH3) (p <0.01), confirming NET inhibition, consistent with recent IgAV-NET mechanistic studies.

Conclusion: By synergizing network pharmacology, 4D-FastDIA proteomics, and experimental validation, this study pioneers the demonstration that ZDZX alleviates IgAV via multi-target inhibition of NET-driven thromboinflammation.

Keywords: anti-inflammatory, anti-NETs formation, immunoglobulin A vasculitis, network pharmacology, 4D-FastDIA proteomic, traditional Chinese medicine

Introduction

Immunoglobulin A vasculitis (IgAV), also referred to as Henoch-Schönlein purpura, is a systemic small-vessel vasculitis primarily affecting children, with an incidence rate ranging from 3 to 55.9 per 100,000 children, demonstrating significant geographic and seasonal variations (higher in autumn/winter).[1,2] The condition is typically characterized by palpable purpura, gastrointestinal involvement (abdominal pain/bleeding), arthralgia, and renal impairment, with 20–60% of patients progressing to IgA vasculitis nephritis (IgAVN) – a critical prognostic determinant.[1–4] Evidence suggests that the incidence of IgAV has been increasing, potentially attributable to alterations in social environments and food contamination, which negatively impact patients' physical and psychological well-being.[1,2,5]

Received: 2 March 2025
Accepted: 28 June 2025
Published: 7 July 2025

Pathogenetically, IgAV is driven by aberrantly glycosylated galactose-deficient IgA1 (Gd-IgA1) forming immune complexes that deposit in the walls of small blood vessels, triggering complement activation (C3) and neutrophil recruitment.[1,2,6] This phenomenon is accompanied by an intensified infiltration of immune cells, particularly neutrophils, at sites of inflammation. Emerging evidence highlights the pivotal role of neutrophil extracellular traps (NETs) in amplifying vascular injury. IgA-IC binding to neutrophils via FcαRI primes neutrophils for NETosis, even at subthreshold activation levels, thereby exacerbating endothelial damage through chromatin release, proteolytic enzymes (eg, myeloperoxidase), and reactive oxygen species (ROS).[1,6,7] Notably, NETs interact synergistically with complement activation: C3a and C5a enhance NETosis, while NET-derived histones further activate the complement cascade, creating a feedforward loop that perpetuates inflammation.[8] This interplay is particularly evident in perivascular tissues, where NETs colocalize with IgA-coated neutrophils and activated endothelial cells, upregulating ICAM-1 and disrupting endothelial barrier.[9] Current therapies for IgAV focus on symptom management but fail to address NETosis-driven pathology.[10,11] Although these treatments can alleviate symptoms, they show limited efficacy in preventing renal progression (30–40% treatment resistance), and associated with substantial adverse effects.[10,12] Chronic corticosteroid use induces impairing calcium absorption and hindering bone development in 15–25% of pediatric patients due to calcium metabolism disruption.

Traditional Chinese medicine (TCM) is recognized as a valuable alternative and complementary approach for managing IgAV, supported by its extensive historical foundation. Recent research has increasingly emphasized the benefits of TCM, including its anti-inflammatory, antioxidant, and anti-tumor properties, along with its generally favorable safety profile and low incidence of adverse effects. Zidian Zhenxiao granule (ZDZX), a TCM formula comprising nine herbal components listed in Table 1, has been employed for over three decades to address IgAV in children at the Affiliated Hospital of Changchun University of Chinese Medicine. Previous investigations have demonstrated that ZDZX is effective in managing Henoch-Schönlein purpura (HSP, also referred to as IgAV), as it reduces disease duration, facilitates the healing of skin lesions and mitigates the risk of renal complications.[13,14] ZDZX, a multi-component Chinese herbal formula, was selected for its dual capacity to disrupt NET-driven pathology and preserve endothelial integrity. Key components include Flavonoid glycosides (Baicalin, Wogonoside, Oroxylin A-7-O-β-D-glucuronide), which quench mitochondrial ROS and suppress neutrophil hyperactivation and NET formation.[15] 6-O-Methylscutellarin (Scutellarin derivative) and Apigenin 7-O-glucoside downregulate ICAM-1 expression, collectively mitigating NET-induced microvascular injury.[15,16] These pharmacological properties align with the pathobiology of IgAV, positioning ZDZX as a rational candidate for NETosis-targeted intervention.

To gain a comprehensive understanding of the therapeutic mechanism of ZDZX in IgAV, we implemented an integrated multi-omics strategy combining network pharmacology and proteomics. Initially, the chemical composition of ZDZX was analyzed by UHPLC-QE-MS technology, followed by the construction of a multidimensional "herb-compound-target-

Table 1 The Composition of ZDZX

Chinese Herbal Name	Botanical Name	Medicinal Parts	Item Number (Production Area)	Ratio
Zicao	*Arnebia guttata* Bunge	Roots	(Xinjiang Uygur, China)	5
Baiwei	*Cynanchum versicolor* Bge.	Roots	(Anhui, China)	10
Dihuang	*Rehmannia glutinosa* Libosch.	Roots	(Henan, China)	10
Mudanpi	*Paeonia* × *suffruticosa* Andr.	Epidermis	(Anhui, China)	6
Baixianpi	*Dictamnus dasycarpus* Turcz.	Root barks	(Liaoning, China)	10
Huangqin	*Scutellaria baicalensis* Georgi	Roots	(Inner Mongolia, China)	10
Qiancao	*Rubia Cordifolia* L.	Roots	(Henan, China)	10
Jixueteng	*Spatholobus Suberectus* Dunn	Stems	(Guangxi, China)	15
Cebaiye	*Platycladus orientalis* (L.) Franco	Leaves	(Henan, China)	10

pathway" interaction network to predict potential therapeutic targets. Subsequently, a gliadin-induced IgAV mouse model was established, differentially expressed proteins (DEPs) were screened using proteomics, GO and KEGG pathway enrichment analysis were performed.[17] Experimental validation further assessed the regulation of key inflammatory factors and markers of coagulation function in animal models. The synergy of network pharmacology and proteomics offers distinct advantages: the former delineates the polypharmacological characteristics of traditional Chinese medicine through multi-compound/multi-target/multi-pathway mapping, whereas quantitative proteomics dynamically captures disease-associated protein alterations, bridging mechanistic insights with clinical applicability.[18,19] The study finally identified 10 core targets (including PTGS2, MMP2, MPO, etc) and 3 key pathways (Complement and coagulation cascades, the TNF signaling pathway, IL-17 signaling pathway). Notably, ZDZX exerts therapeutic effects by modulating complement activation and suppressing NETosis, mechanisms critically linked to IgAV pathogenesis. These findings not only clarify ZDZX's anti-inflammatory and immunoregulatory properties but also provide a framework for developing targeted therapies against IgAV.

Materials and Methods

Drugs

ZDZX, a TCM formula comprising nine herbal ingredients listed in Table 1, was verified using the Plant List database (http://www.theplantlist.org). ZDZX was procured from the Affiliated Hospital of Changchun University of Chinese Medicine. The nine herbs were combined and subjected to two rounds of decoction, with each process involving the addition of eight times the volume of distilled water for 2 h, followed by filtration. The aqueous extract obtained from ZDZX was subsequently concentrated using an evaporator (IKA, Germany). Dexamethasone (Dex) was supplied by Zhejiang Xianju Pharmaceutical Co., Ltd.

Identification of ZDZX

UHPLC-QE-MS/MS Analysis of ZDZX

The compounds present in ZDZX were identified through the use of a Dionex Ultimate 3000 UHPLC system (Thermo Corporation, United States) coupled with a Q Exactive high-resolution mass spectrometer (Thermo Fisher Scientific, Shanghai, China). A 3 mL aliquot of ZDZX extract (4 mg/mL) was introduced into a Zorbax Eclipse C18 column (1.8 μm, 2.1 mm × 100 mm) within the UHPLC system. The system was operated at a flow rate of 0.3 mL/min, with the column and autosampler temperatures maintained at 30°C and 4°C, respectively. The mobile phase comprised A: 0.1% formic acid solution and B: pure acetonitrile. The gradient elution program was as follows: 0–2 min, 95% B; 2–6 min, 30% B; 6–7 min, 30% B; 7–12 min, 78% B; 12–14 min, 78% B; 14–17 min, 95% B; 17–20 min, 95% B; 20–21 min, 5% B; and 21–25 min, 5% B. Analyses were conducted in both positive and negative ion scanning modes. Feature peak extraction was performed using Compound Discoverer 3.3, and substance identification was carried out with the Thermo mzCloud online database and the Thermo mzValut local database.

High-Performance Liquid Chromatography (HPLC) Analysis of ZDZX

Baicalin, Oroxylin A-7-O-glucuronide, Pectolinarigenin, and Mirificin were primarily identified through HPLC. The ZDZX extract was transferred into a 50 mL centrifuge tube, and 50 mL of 50% methanol was added. Ultrasonic extraction was performed for 10 min, followed by centrifugation at 8000 rpm for 5 min. The resulting supernatant was filtered through a 0.22 μm microporous membrane and then analyzed by an Agilent 1260 liquid chromatography system. The samples were made to pass through a SHISEIDO C18 column (4.6 mm × 250 mm, 5 μm) under a mobile phase comprising methanol (marked as A) and 0.1% phosphoric acid (marked as B) at 30°C, with a flow rate of 1.0 mL/min. The HPLC signal was subsequently detected at a wavelength of 280 nm. The supernatant was processed using the same method, filtered through a 0.22 μm microporous membrane, and analyzed with an Agilent 1290–6470 liquid chromatography system. Using 0.1% phosphoric acid (mobile phase A) and acetonitrile (mobile phase B), An Agilent C18 column (2.1 mm × 100 mm, 1.7 μm) was used to pass the samples through at 30°C, with a flow rate of 0.3 mL/min.

Network Pharmacology Analysis

This study utilized a network pharmacology approach to comprehensively investigate the mechanism of action of ZDZX in the treatment of IgA vasculitis (IgAV). Initially, ZDZX's chemical constituents were identified through the TCMSP and prior UHPLC-QE-MS/MS data, selecting potential active ingredients with oral bioavailability (OB) ≥ 30% and drug-likeness (DL) ≥ 0.18.[20] The targets of these components were subsequently predicted using the SwissTargetPrediction and PharmMapper online tools, while genes associated with the targets were retrieved from the UniProt protein database. A research dataset was then constructed by querying "Immunoglobulin A vasculitis" and "Henoch-Schönlein purpura" in the Comparative Toxicogenomics Database (CTD), Genecards, and Online Mendelian Inheritance in Man (OMIM) database,[21–23] identifying the top 400 target genes associated with IgAV based on higher inference scores. GO and KEGG pathway enrichment analyses were performed on the intersection of drug and disease targets using the DAVID web server, and significant pathways with P-values < 0.05 were selected. Proteins were identified through BLAST alignment (blastp, e-value ≤ 1e-4) and annotated based on the highest-scoring matches. A bubble plot was generated using a bioinformatics visualization tool to display the enrichment results. Furthermore, human overlapping targets were queried in the STRING database with a minimum interaction score of "high confidence (0.700)" to construct a "herb-component-target-disease-documentation" network. The top 10 hub genes were identified by ranking nodes according to their network attributes using the cytoHubba plugin in CytoScape 3.8.2 software, thereby clarifying the complex interactions among herbs, components, diseases, literature, and targets.[24] Three topological criteria—degree, betweenness centrality, and closeness centrality—were applied to filter the network's active ingredients.

The Network Pharmacology research content is exempt from ethical approval based on national legislation, specifically item 1 and item 2 of Article 32 of the Measures for Ethical Review of Life Science and Medical Research Involving Human Subjects (promulgated on February 18, 2023, China).

Animals and IgAV Models

A total of 120 male C57BL/6J mice (21–24 g, aged 6 weeks) were allocated randomly into six experimental groups: Sham, Model, ZDZX-L (2.97 g/kg/day), ZDZX-M (5.95 g/kg/day), ZDZX-H (11.9 g/kg/day), and Dex (0.84 g/kg/day). The administered doses were calculated using human-to-animal equivalent dose conversion ratios. The selection of gliadin and Indian ink aligns with established protocols for modeling IgA vasculitis (IgAV), particularly in replicating immune complex deposition and systemic inflammation. Gliadin, a well-characterized antigen, induces IgA1 overproduction—a hallmark of IgAV pathogenesis—while Indian ink blocks the reticuloendothelial system, prolonging immune complex circulation and mimicking human disease mechanisms.[25] All groups, with the exception of the Sham group, were subjected to weekly injections of Indian Ink (0.4 mg per 10 g body weight) over a period of three weeks. Subsequently, each mouse was intragastrically administered 0.5 mL of a 1 mg/mL Gliadin solution (Sigma, USA) dissolved in 6 mmol/L HCl twice daily for 11 weeks. Additionally, a daily tail vein injection, consisting of 0.1 mL of 10 mg/mL gliadin combined with 0.1 mL of PBS, was conducted over three days. Mice exhibiting purpura skin, indicative of successful modeling, were selected for further experimentation. During the subsequent two weeks, all groups, excluding the Sham and Model groups, received daily intragastric administration of the respective medications at designated doses, while the Sham and Model groups were given an equivalent volume of saline. The schematic representation of the experimental design is depicted in Figure 4A. At the conclusion of the 16th week, all mice were euthanized, and blood as well as kidney samples were collected for subsequent analyses.

C57BL/6 mice were obtained from Changchun City Yisi Experimental Animal Technology Limited Liability Company (License No. SCXK [Ji] 2020-0002, Changchun, China) and housed in a designated pathogen-free environment. Access to laboratory chow and water was provided as and libitum. All experimental procedures involving animals complied with the regulations stipulated by the Animal Ethics Committee of Changchun University of Chinese Medicine (No. 20220612).

Peripheral Blood Collection and Analysis

Whole blood samples obtained in EDTA tubes were analyzed utilizing an Idexx Procyte Dx Hematology Analyzer (Idexx Laboratories). A manual white blood cell differential was conducted on 100 cells derived from a blood smear stained with Accustain Wright-Giemsa stain (Sigma-Aldrich, USA).

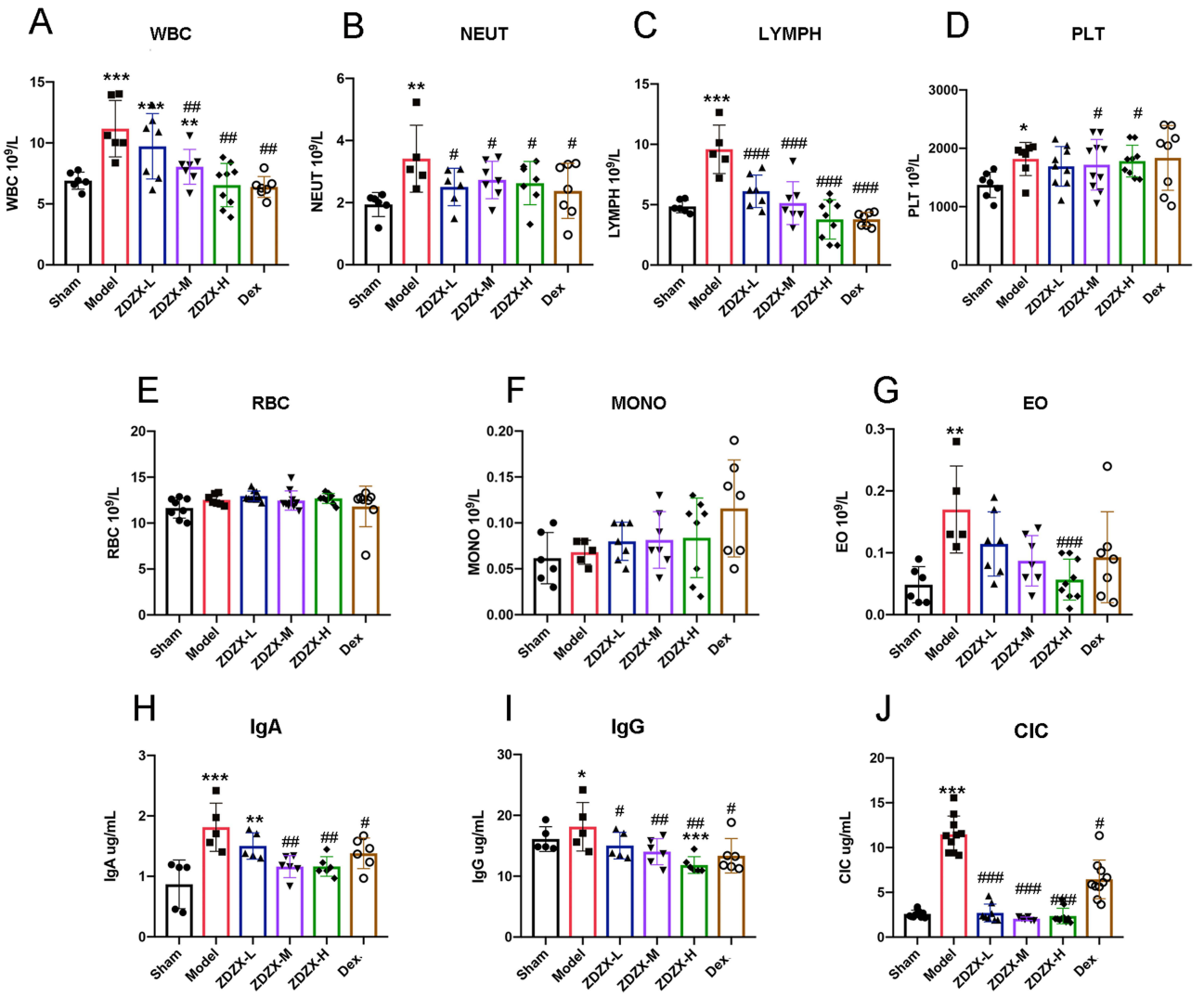

Figure 1 ZDZX improves blood parameters and levels of immune complex associated with IgAV. (**A**) peripheral blood count. WBC, White blood cell count. **P < 0.01, ***P < 0.001 versus the Sham group; ##P < 0.01 versus the Model group, n=6-8. (**B**) NEUT, Neutrophils. **P < 0.01 versus the Sham group; #P < 0.05 versus the Model group, n=6-8. (**C**) LYMPH, Lymphocyte count. ***P < 0.001 versus the Sham group; ###P < 0.001 versus the Model group, n=6-8. (**D**) PLT, Platelet count. *P < 0.05, versus the Sham group; #P < 0.05 versus the Model group, n=6-8. (**E**) RBC, Red blood cell count. (**F**) MONO, monocytes count. (**G**) EO, Eosinophils count. **P < 0.01 versus the Sham group; ###P < 0.05 versus the Model group, n=6-8. (**H–J**) immune complex in serum. *P < 0.05, **P < 0.01, ***P < 0.001 versus the Sham group; #P < 0.05, ##P < 0.01, ###P < 0.001 versus the Model group, respectively, n=6-8. Data are expressed as means ± SD.

Examination of Histopathology

Mouse kidney tissues were preserved in 10% paraformaldehyde (Solarbio, Beijing, China) overnight and subsequently processed into paraffin blocks. Representative images were acquired through fluorescence inverted microscopy (Nikon, Tokyo, Japan).

Immunofluorescence (IF) and Immunohistochemistry (IHC)

For IF, kidney sections were fixed with 5% BSA in PBS for 30 min at 24°C to prevent further activity. Later, sections were incubated with primary antibodies (anti-IgA, Santa Cruz, USA) in 1% BSA overnight at 4°C. Next, HRP-conjugated secondary antibodies were applied to the samples for 2 h in the dark at room temperature. Finally, the DAPI solution was added to all sections and incubated for 10 min. Images were captured using a confocal laser scanning microscope (Nikon, Tokyo, Japan) from three random fields of view.

https://doi.org/10.2147/JIR.S522082

Immunohistochemical (IHC) staining was conducted to analyze myeloperoxidase (MPO) expression using an anti-MPO antibody (Proteintech, China). Positive area intensities were quantified using ImageJ software (NIH, Bethesda, MD). Three sections from each group were analyzed.

Measurement of Myeloperoxidase Enzyme Activity

Neutrophils are known to contain abundant granule enzyme MPO, whose activity is widely utilized as an indicator of neutrophil infiltration.[26] Kidney tissues were homogenized in cold PBS at a ratio of 1:10 (g/mL) and subsequently centrifuged at 12,000 rpm for 15 min at 4°C. Following the removal of supernatants from the tissue homogenates, 10 μL of the remaining solution was dispensed into a 96-well plate and combined with 100 μL of TMB (Beyotime, Beijing, China) at 37°C for 5 min. The reaction was terminated with 2M H2SO4 and quantified at 450 nm using a microplate reader.

ELISA

For hematologic analysis, blood samples were drawn into EDTA tubes, while serum separator tubes were utilized for immunoglobulin testing. Blood was extracted from the orbital sinus, allowed to clot at 4°C for 30 min, and subsequently centrifuged at 3500 r/min for 10 min. The resulting supernatant was collected and stored at −80°C. Serum concentrations of IgA, IgG, and CIC were quantified using ELISA kits. Specifically, IgA and IgG ELISA kits were procured from Jiancheng (Nanjing, China), while CIC ELISA kits were sourced from CUSABIO (Wuhan, China).

Kidney tissue homogenates were prepared, and supernatants were obtained, as outlined in the MPO enzyme activity section. Commercial ELISA kits (Meimian, Nanjing, China) were employed to determine the levels of IL-1β, IL-6, and IL-17, while MPO-DNA and Cit-H3 concentrations were measured using ELISA kits from Elabscience (Wuhan, China).

RT-qPCR-Mediated Analysis

For RT-qPCR, total RNA was isolated from tissue samples utilizing an RNA Extraction Kit (Takara, Tokyo, Japan). The isolated RNA was subsequently reverse-transcribed into cDNA with the RT First Strand cDNA Synthesis Kit (Servicebio, Wuhan, China) according to the manufacturer's protocol. Quantitative PCR was conducted with FastStart Universal SYBR Green Master (Roche, Germany) to assess relative mRNA expression levels using specific primers listed in Table 2. Primer sequences were retrieved from PrimerBank (https://pga.mgh.harvard.edu/primerbank/), and synthesis of the primers was carried out by Comate Bioscience Co., Ltd. Relative expression levels were determined by the 2-ΔΔCT method, with GAPDH serving as the internal control.

Proteomic Analysis

To investigate the protein targets and biological pathways associated with the therapeutic effects of ZDZX on IgAV, 4D-FastDIA proteomics was employed. The analysis was carried out by Jingjie PTM BioLab Co., Ltd. (Hangzhou, China). Mouse kidney tissues were harvested immediately following euthanasia and processed within tissue cassettes. Proteins exhibiting a fold change exceeding 1.2 or falling below 0.83 were categorized as differentially expressed.

Table 2 Primer Sequence

Gene	Primer Sequence
GAPDH	Forward Primer: AATGGATTTGGACGCATTGGT Reverse Primer: TTTGCACTGGTACGTGTTGAT
IL-6	Forward Primer: CTGCAAGAGACTTCCATCCAG Reverse Primer: AGTGGTATAGACAGGTCTGTTGG
IL-1β	Forward Primer: GAAATGCCACCTTTTGACAGTG Reverse Primer: TGGATGCTCTCATCAGGACAG
IL-17	Forward Primer: TCAGCGTGTCCAAACACTGAG Reverse Primer: CGCCAAGGGAGTTAAAGACTT

Bioinformatics analyses, including volcano plot generation, GO enrichment, and KEGG pathway analysis, were conducted to elucidate the mechanisms underlying ZDZX's therapeutic action against IgAV.

Statistical Analysis

The data were expressed as the mean ± standard deviation. Statistical comparisons among groups for quantitative data were conducted using one-way ANOVA followed by a post-hoc LSD test. GraphPad Prism version 8 (LaJolla, CA, USA) was employed for statistical analysis, and results from at least three independent experiments were considered. A P-value of < 0.05 was regarded as statistically significant.

Results

Analysis of the Chemical Composition of ZDZX

The chemical composition of ZDZX was analyzed through UHPLC-QE-MS to acquire retention time and mass spectrometry data for each compound. Based on the evaluation scores, 19 components were identified with high confidence, including baicalin, oroxylin A-7-O-β-D-glucuronide, mirificin, pectolinarigenin, paeoniflorin, and apigenin 7-O-glucuronide in Figure 2A, B and Table 3.

To ensure the quality and consistency of ZDZX, the "Similarity Evaluation System for Chromatographic Fingerprints of Traditional Chinese Medicine 2004A Version", developed by the Chinese Pharmacopoeia Commission, was utilized. This software serves as an essential tool for generating and comparing chromatographic fingerprints, ensuring consistency in the chemical composition of ZDZX across different batches. Six batches of ZDZX (S1-S6) were prepared, and control fingerprints were generated using the software. Reference peaks, including oroxylin A-7-O-β-D-glucuronide, mirificin, pectolinarigenin, and baicalin, were selected due to their stable chemical properties, moderate peak areas, and retention times. The similarity comparison of chromatographic peaks across the six batches demonstrated a detection range of 0.926 to 0.992, indicating a high degree of similarity in Figure 2C and D. This similarity is pivotal in maintaining the therapeutic efficacy and safety of the medicine. Furthermore, the six batches of ZDZX retained the primary chemical components of the nine traditional Chinese herbs, confirming the reproducibility of ZDZX preparation and the stability of its active components.

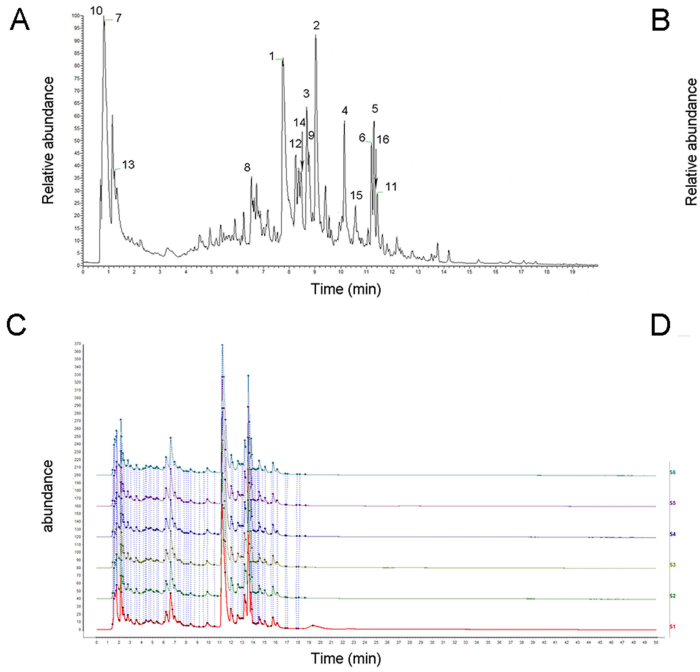

No.	S1	S2	S3	S4	S5	S6	S0
S1	1.00	0.992	0.936	0.940	0.985	0.984	0.989
S2	0.992	1.00	0.931	0.941	0.992	0.992	0.991
S3	0.936	0.931	1.00	0.962	0.928	0.926	0.965
S4	0.940	0.941	0.962	1.00	0.941	0.943	0.973
S5	0.985	0.992	0.928	0.941	1.00	0.996	0.990
S6	0.984	0.992	0.926	0.943	0.996	1.00	0.990
S0	0.989	0.991	0.965	0.973	0.990	0.990	1.00

Figure 2 Chemical composition analysis of ZDZX. (**A**) The total ions current (TIC) in positive ion mode; (**B**) The TIC in negative ion mode. (**C**) HPLC fingerprint of 6 batches of samples (S1, S2, S3, S4, S5 and S6). (**D**) Similarity assessment of 6 batches.

https://doi.org/10.2147/JIR.S522082

Table 3 Chemical Composition Analysis of ZDZX

Number	RT (min)	Identification	Formula	CAS_num	Class	*m/z*	Error (ppm)	Adducts
1	7.759	Baicalin	C21 H18 O11	21967-41-9	Flavonoids	446.08443	−1.08	[M+H]+
1	8.363	Baicalin	C21 H18 O11	21967-41-9	Flavonoids	446.08551	1.34	[M+H]−
2	9.033	Wogonoside	C22 H20 O11	51059-44-0	Flavonoids	460.10003	−1.16	[M+H]+
3	8.686	Oroxylin A-7-O-β-D-glucuronide	C22 H20 O11	36948-76-2	Flavonoids	460.09999	−1.24	[M+H]+
3	9.027	Oroxylin A-7-O-β-D-glucuronide	C22 H20 O11	36948-76-2	Flavonoids	460.10124	1.48	[M+H]−
4	10.139	Baicalein	C15 H10 O5	491-67-8	Flavonoids	270.05257	−0.94	[M+H]+
5	11.283	Chrysosplenetin B	C19 H18 O8	603-56-5	Flavonoids	374.09966	−1.37	[M+H]+
6	11.194	Wogonin	C16 H12 O5	632-85-9	Flavonoids	284.06804	−1.52	[M+H]+
7	0.825	DL-Arginine	C6 H14 N4 O2	7200-25-1	Carboxylic acids and derivatives	174.11157	−0.58	[M+H]+
8	6.534	Puerarin apioside	C26 H28 O13	103654-50-8	Prenol lipids	548.15257	−0.77	[M+H]+
8	6.53	Puerarin apioside	C26 H28 O13	103654-50-8	Prenol lipids	548.15376	1.4	[M+H]−
9	8.788	6-O-Methylscutellarin	C22 H20 O12	31105-76-7	Flavonoids	476.09505	−0.9	[M+H]+
10	0.789	Choline	C5 H13 N O	62-49-7	Organonitrogen compounds	103.10004	3.15	[M+H]+
11	11.417	Oroxylin A	C16 H12 O5	480-11-5	Flavonoids	284.06798	−1.74	[M+H]+
12	8.265	Syringetin	C17 H14 O8	4423-37-4	Flavonoids	346.06841	−1.33	[M+H]+
13	1.223	Adenosine	C10 H13 N5 O4	58-61-7	Purine nucleosides	267.09645	−1.13	[M+H]+
14	8.765	Daidzein-7-O-glucuronide	C21 H18 O10	38482-80-3	Isoflavonoids	430.08968	−0.74	[M+H]+
14	8.792	Daidzein-7-O-glucoside	C21 H18 O10	38482-80-3	Isoflavonoids	430.09051	1.19	[M+H]−
15	10.575	Paeonol	C9 H10 O3	552-41-0	Organooxygen compounds	166.06293	−0.39	[M+H]+
16	11.346	Pectolinarigenin	C17 H14 O6	520-12-7	Flavonoids	314.07859	−1.44	[M+H]+
16	11.279	Pectolinarigenin	C17 H14 O6	520-12-7	Flavonoids	314.07938	1.09	[M+H]−
17	6.239	Paeoniflorin	C23 H28 O11	23180-57-6	Prenol lipids	480.16391	1.56	[M+H]−
18	5.352	(+)-Catechin hydrate	C15 H14 O6	225937-10-0	Flavonoids	290.07936	1.12	[M+H]−
19	7.754	Apigenin 7-O-glucoside	C21 H18 O11	29741-09-1	Flavonoids	446.08534	0.96	[M+H]−

Network Analysis of the Active Component in ZDZX

The chemical constituents of ZDZX were analyzed through mass spectrometry and identified by comparison with the TCMSP. A total of 563 chemical constituents were detected. Furthermore, 1266 IgA-related targets were retrieved by searching "Disease and IgA vasculitis" across three databases: GeneCards, CTD, and OMIM. Following data intersection and duplicate removal using Excel, 108 unique target genes were identified and subsequently verified through the UniProt database.

To explore the potential targets of ZDZX in IgAV, 1039 ZDZX-related targets and 108 IgAV-associated targets were mapped onto Venn diagrams. A total of 46 overlapping targets were subsequently identified as potential therapeutic targets for ZDZX in the treatment of IgAV, as depicted in Figure 3A. As illustrated in Figure 3B, CytoScape was employed to construct a "herbs-components-targets-disease" network, providing insight into the comprehensive effects of ZDZX. Key targets of ZDZX in IgAV treatment were further analyzed by generating a protein-protein interaction (PPI) network through the String platform, with the 46 overlapping targets assessed using Cytoscape. Figure 3C depicts the PPI network, comprising 46 nodes and 247 edges. The degree values are represented by a color gradient ranging from yellow to purple, indicating increasing values. Larger nodes denote higher degree values, as visualized by the color scale. The top 10 hub genes, ranked by degree value, were identified as critical targets, including PTGS2, PPARG, CYCS, MMP2, VCAM1, GSK3B, MPO, CYP3A4, MAPK14, and KDR.

To elucidate the functions of ZDZX in the treatment of IgAV, overlapping targets were analyzed, revealing 28 entries associated with biological processes (BP) ($P < 0.05$). Figure 3D highlights the top 10 enriched terms within the BP category, primarily encompassing collagen metabolic processes, collagen catabolic processes, and the regulation of

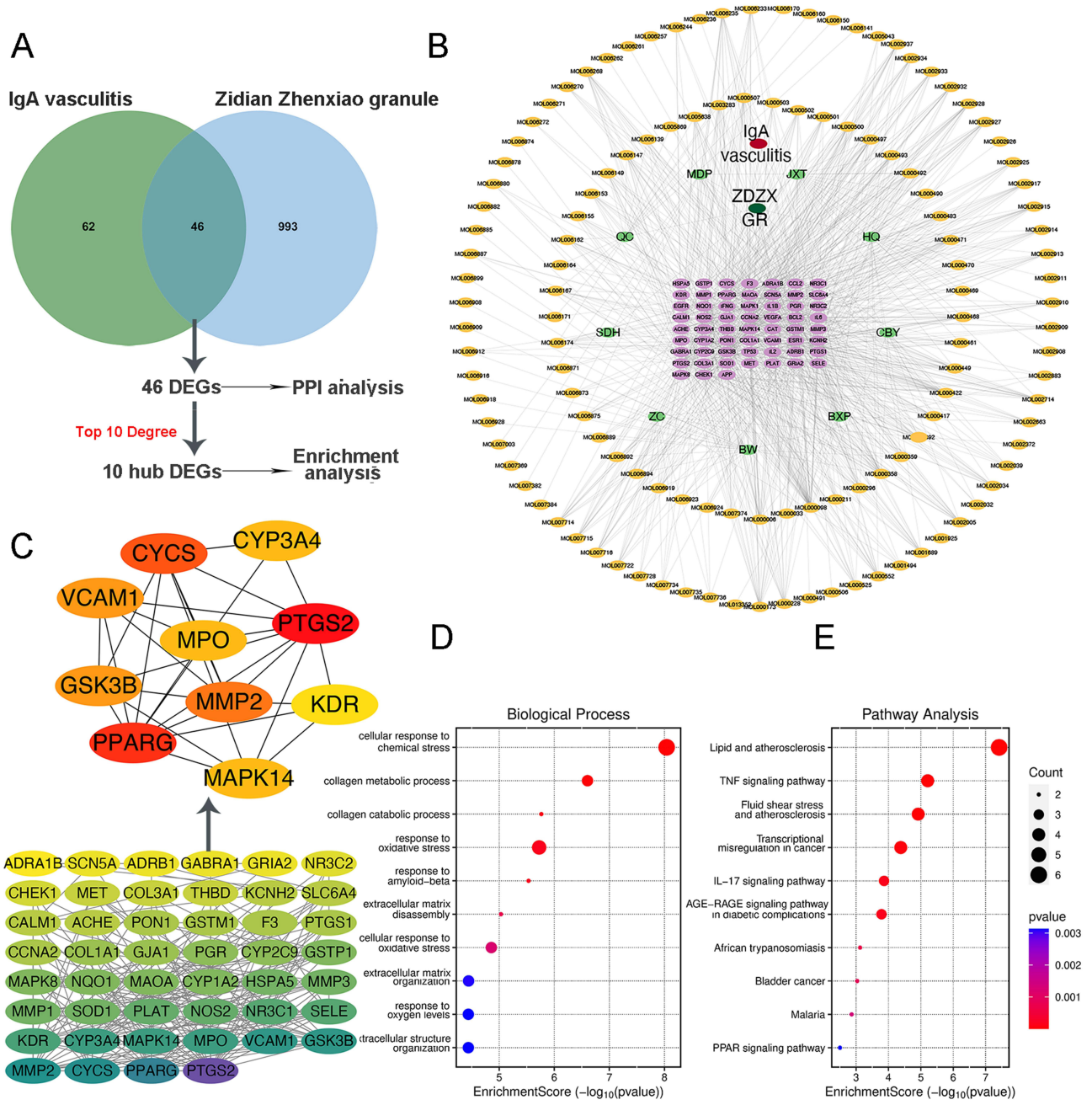

Figure 3 Identification of the potential targets and components of ZDZX in the treatment of IgAV. (**A**) Venn diagram of the potential targets in ZDZX and the therapeutic targets for IgAV. (**B**) Herbs-Compound-Disease-Target-Decoction Network. The outermost yellow hexagon circle represents the active ingredient contained in ZDZX, and the middle green triangle denotes the herbs, the red ellipse represents the disease, the dark green represents the decoction, and pink diamond denotes the therapeutic targets. (**C**) The screening process of PPI network topology. (**D**) GO pathway enrichment analysis of 46 IgAV treatment targets in ZDZX. The top 10 significantly enriched ($P < 0.05$) terms in BP of GO analysis were selected; (**E**) KEGG pathway enrichment analysis of 46 IgAV treatment targets in ZDZX. The top 10 KEGG pathways with significantly enriched ($P < 0.05$) were selected. The Y-axis represents the main pathway, and the X-axis represents the enrichment score.

inflammatory responses. These findings indicate that ZDZX may modulate gene expression by influencing collagen production and functionality, thereby suppressing the inflammatory process in IgAV. Based on the results of GO analysis, ZDZX appears to contribute to IgAV treatment by regulating BPs and molecular functions associated with immune responses and inflammation. Moreover, ZDZX treatment of IgAV was found to enrich 19 pathways ($P < 0.05$). The top 10 KEGG pathways, illustrated in Figure 3E, include the TNF signaling pathway, IL-17 signaling pathway, and AGE-RAGE signaling pathway in diabetic complications, among others. These results imply that ZDZX may alleviate the

https://doi.org/10.2147/JIR.S522082

pathological mechanisms of IgAV through multiple avenues, including the reduction of inflammation, immune system regulation, and enhancement of vascular function.

ZDZX Improves Skin State and Renal Function in IgAV Mice

To establish an experimental animal model of IgAV, gliadin was employed as a dietary antigen, and Indian ink was administered to impair the reticuloendothelial system, thereby providing continuous stimulation to the mucosal immune system. The modeling workflow is depicted in Figure 4A.

Mice in the sham group exhibited normal skin color and activity, with no bleeding spots observed throughout the experimental period. In the model group, 5 out of 10 mice developed sporadic, needle-tip-sized bleeding spots without surrounding swelling, consistent with the clinical features of IgAV in Figure 4B. In all groups, except the sham group, the percentage of bleeding patches ranged between approximately 50% and 70%. By the 7th day following treatment, bleeding spots had resolved in the ZDZX-H and Dex groups, while partial resolution was observed in the ZDZX-L/M group. By the 14th day, bleeding spots had entirely disappeared in all groups except the ZDZX-L group, with no new occurrences recorded during the treatment period.

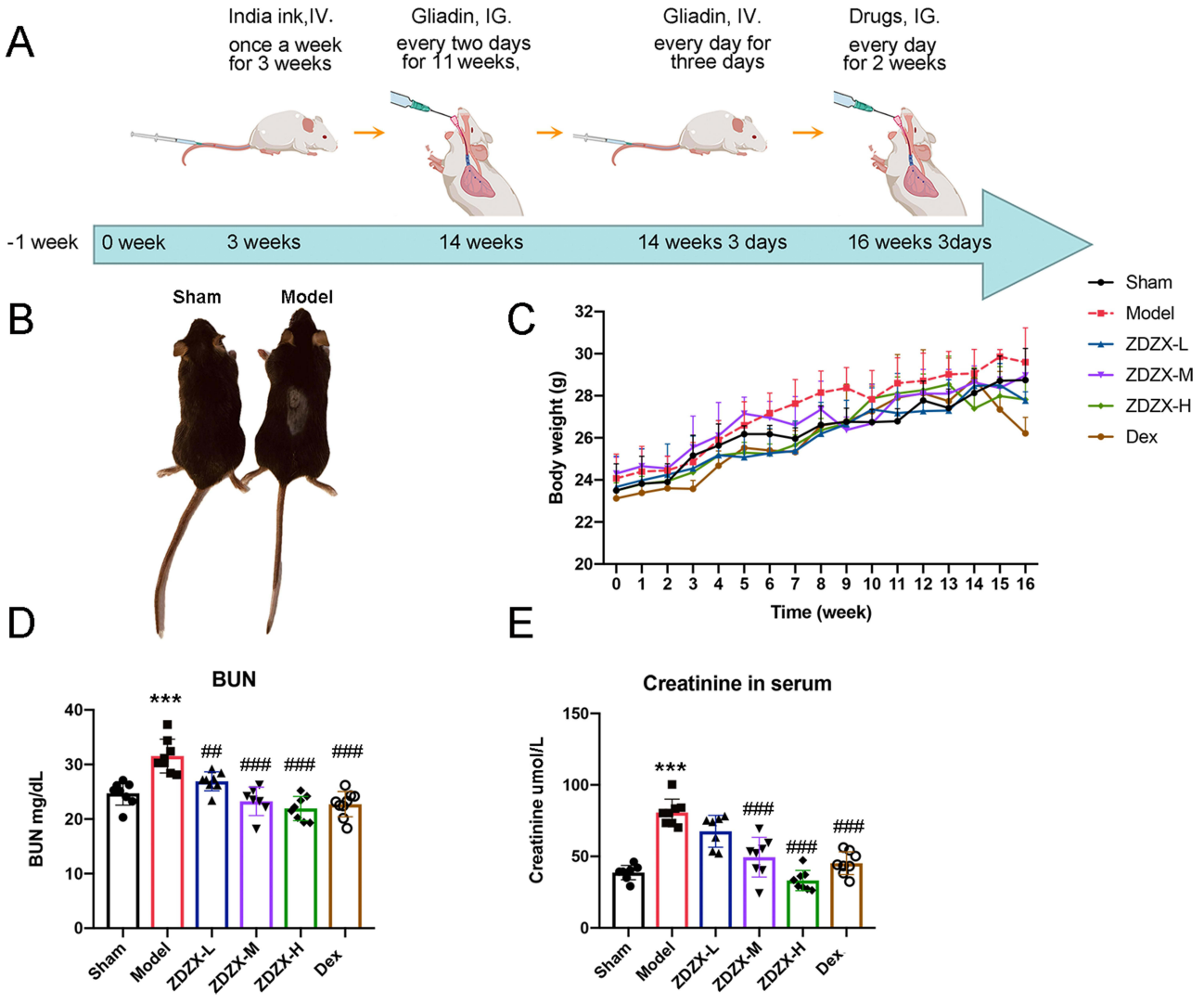

Figure 4 ZDZX improves renal function. (**A**) Experimental design for the Gliadin-induced IgAV model. (**B**) On the 14th week, the mice were sacrificed, and their skin changed. (**C**) The weekly weight changes the mean value in each group. (**D**) BUN and (**E**) Creatinine in the mouse serum, n=6-8. ***P < 0.001 versus the Sham group; ##P < 0.01, ###P < 0.001 versus the Model group, respectively. Data are expressed as means ± SD.

 https://doi.org/10.2147/JIR.S522082

In terms of body weight, mice did not display significant weight gain during the Indian ink injection phase (0–3 weeks), suggesting that the initial administration of Indian ink did not induce severe systemic effects. During the gliadin gavage period (3–14 weeks), mice across all groups maintained normal growth, exhibiting no significant differences relative to the sham group. This stable growth indicates that the treatment was well-tolerated and did not adversely affect the overall health of the mice. During the drug treatment phase (14–16 weeks), mice in the Dex and ZDZX-L groups experienced slight weight loss, though no significant differences were observed compared to the sham group in Figure 4C. These observations validate the reliability of the experimental results and confirm the overall health of the animals throughout the study.

Renal function parameters, particularly BUN and creatinine levels, were evaluated to assess the impact of ZDZX on kidney health in IgAV mice. As illustrated in Figure 4D and E, serum BUN and creatinine levels were markedly elevated in the model group compared to the sham group ($P < 0.01$), confirming the successful establishment of renal impairment. Treatment with ZDZX at all doses significantly reduced serum BUN levels in IgAV mice relative to the model group ($P < 0.01$). Furthermore, medium and high doses of ZDZX significantly decreased serum creatinine levels, suggesting a potential renal-protective effect. These results highlight the therapeutic potential of ZDZX in addressing renal complications associated with IgAV and provide a foundation for subsequent research.

ZDZX Treatment Improves Blood Parameters and Immune Complex Levels in IgAV Mice

Hematological parameters related to IgAV were evaluated through complete blood count analysis in mice. Figure 1A–G demonstrate a significant elevation in peripheral blood parameters, including total white blood cells (WBC), lymphocytes (LYMPH), platelets (PLT), and eosinophils (EO), in the model group compared to the sham group ($P < 0.05$). Treatment with ZDZX and Dex effectively reduced total WBC levels relative to the model group. Among leukocyte subtypes, neutrophils (NEUT) and lymphocytes (LYMPH) showed significant decreases, while monocytes (MONO) and red blood cells remained unchanged. Notably, ZDZX treatment induced a significant reduction in LYMPH count compared to the model group ($P < 0.01$). Medium and high doses of ZDZX were more effective in normalizing PLT counts than the low dose or Dex. Additionally, high doses of ZDZX significantly reduced EO levels compared to the model group ($P < 0.001$). Collectively, these findings indicate that ZDZX and Dex improve specific hematological indices in gliadin-induced IgAV mice.

The impact of ZDZX on immune complex levels in IgAV mice was assessed by measuring serum IgA, IgG, and circulating immune complexes (CIC) using ELISA. Figure 1H–J reveal that the gliadin-induced model group displayed significantly elevated levels of serum IgA, IgG, and CIC compared to the sham group ($P < 0.01$), verifying the successful induction of immune complex-mediated inflammation. Conversely, ZDZX treatment significantly reduced serum IgA, IgG, and CIC levels relative to the model group ($P < 0.01$). This reduction was most pronounced with medium and high doses of ZDZX, suggesting a dose-dependent effect. The decrease in immune complex levels indicates that ZDZX mitigates the inflammatory response and tissue damage associated with IgAV. Histopathological analysis of kidney tissues further corroborated these results. IF staining revealed reduced deposition of ICs in the glomeruli of ZDZX-treated mice compared to the model group in Figure 5B. This reduction in immune complex deposition corresponded with improved renal function, as evidenced by decreased serum BUN and creatinine levels in ZDZX-treated groups in Figure 4D and E.

These findings indicate that ZDZX treatment effectively diminishes immune complex levels and deposition in IgAV mice, thereby contributing to its therapeutic effects on both renal and systemic inflammation. This evidence highlights the potential application of ZDZX as an innovative therapeutic agent for the management of IgAV.

Combined Histopathological Techniques in Assessing Renal Damage in IgAV Mice

To comprehensively evaluate the renal protective effects of ZDZX on immunoglobulin A vasculitis (IgAV)-induced nephropathy, histopathological assessments were systematically performed using H&E, PAS, Masson's trichrome, and immunofluorescence (IF) staining, as illustrated in Figure 5A. In the sham group, glomeruli exhibited intact architecture without pathological alterations in the basement membrane, mesangial cells, interstitial cells, extracellular matrix, or vascular lumens. In contrast, IgAV model mice manifested severe tubular epithelial cell degeneration, characterized by

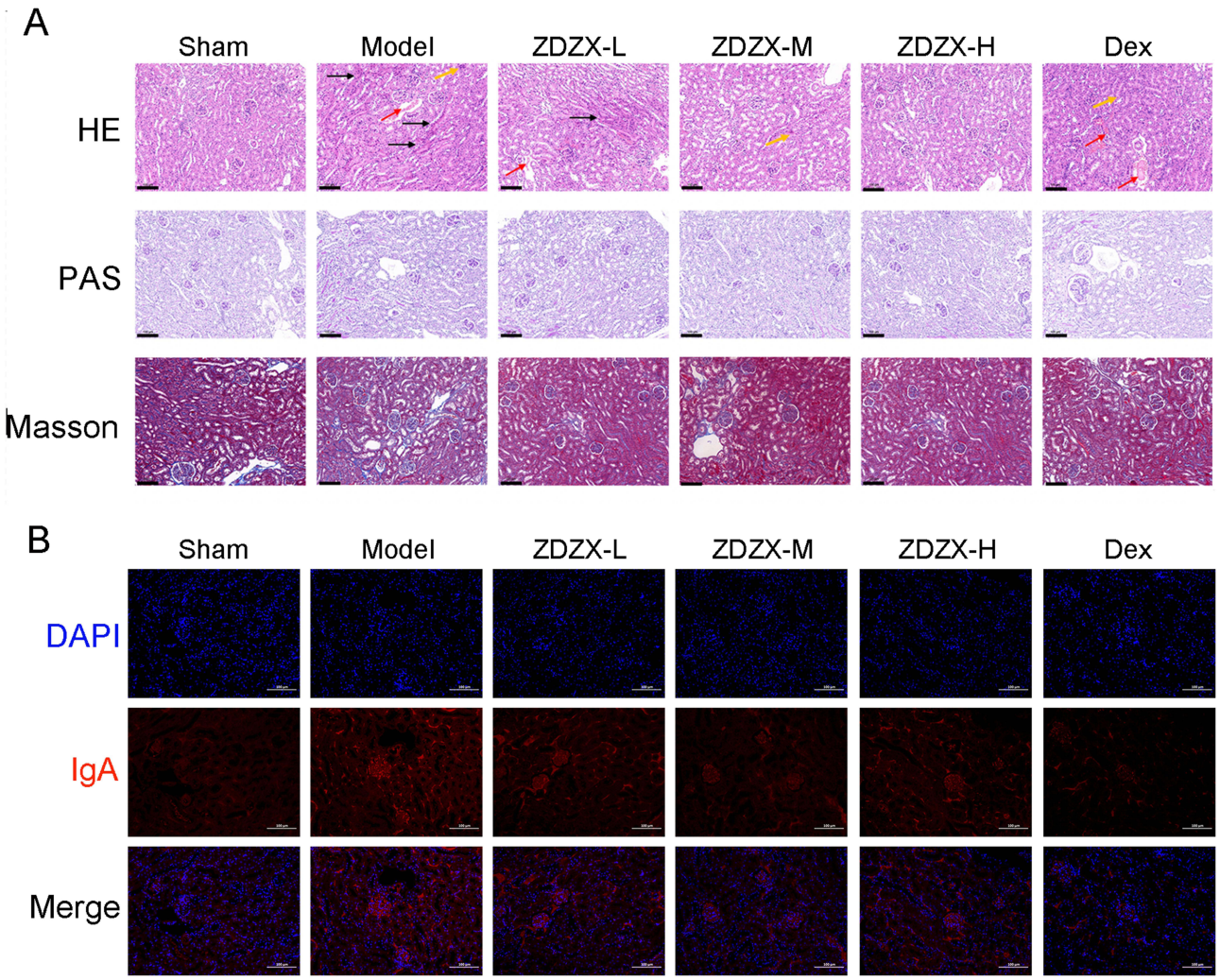

Figure 5 ZDZX attenuated renal-infiltrated associated with IgAV and diminished IgA deposition in the kidney. (**A**) The histopathological changes in the kidney tissue were examined by H&E staining, PAS, and Masson staining; numerous renal tubular epithelial cells were denatured, with eosinophilic flocculent in the lumen (red arrow). The interstitial and glomerular capillaries were congested (black arrows), and representative pictures were shown. Scale bars: 100 μm. (**B**) Immunofluorescence of IgA. IgA was positive in the mesangial region of the glomerulus in the model group. The sham group was negative. Scale bars: 100 μm.

vacuolated cytoplasm and eosinophilic casts within the tubular lumen. Notably, ZDZX treatment at various doses significantly attenuated inflammatory infiltration, preserved the integrity of glomerular structures, clarified vascular loop architecture, normalized glomerular cyst size, and resolved significant tissue bleeding. PAS staining further revealed marked mesangial hypercellularity and matrix expansion in model mice, indicative of immune complex deposition and the associated inflammatory response. These changes were effectively mitigated by ZDZX treatment, with notable reductions in basement membrane thickness. Masson's trichrome staining demonstrated extensive interstitial collagen deposition (blue-stained area: 37.3% ± 1.8% in model group vs 34.1% ± 1.2% in sham group, $P < 0.001$), confirming fibrosis progression. Treatment with ZDZX significantly reduced collagen area to 33.9% ± 1.5% in ZDZX-M group, ($P<0.001$ vs model group), as illustrated in Figure 5A and SFigure 1.

IF analysis revealed IgA deposition within the renal mesangium. In the model group, diffuse granular or massive red fluorescent ICs were observed in both the renal body and cortex. Treatment with ZDZX reduced immune complex deposition, with mild IgA deposition noted in the medium-dose ZDZX group and slightly more pronounced deposition in the high-dose and low-dose ZDZX groups, as illustrated in Figure 5B. The mean fluorescence intensity indicated a significant increase in IgA deposition in the kidneys of model mice compared to sham mice ($P < 0.01$). Conversely,

Table 4 Effect of ZDZX on Renal IgA Deposition in IgAV Mice

Group	Dose (g/kg)	Mean
Sham	–	83.77±9.33
Model	–	100.52±6.39**
ZDZX-L	2.87 g/kg	88.91±13.07
ZDZX-M	5.73 g/kg	85.97±13.94#
ZDZX-H	11.46 g/kg	87.58±12.29
Dex	0.63 mg/kg	80.07±10.96##

Notes: **P < 0.01 versus the Sham group; #P < 0.05, ##P < 0.01 versus the Model group, respectively.

IgA deposition was significantly decreased in the kidneys of medium-dose ZDZX and Dex-treated mice relative to the model group ($P < 0.05$ or $P < 0.01$). These findings are summarized in Table 4.

Through the integration of these histopathological techniques, a comprehensive understanding of renal damage in IgAV mice and the therapeutic effects of ZDZX was achieved. These results highlight the potential of ZDZX in mitigating renal inflammation, immune complex deposition, and fibrosis, thereby providing renoprotective effects.

ZDZX Modulates Proinflammatory Cytokine Levels and Neutrophil Extracellular Traps (NETs) Formation in IgAV Mice

To further elucidate the specific targets and molecular mechanisms underlying the therapeutic effects of ZDZX in IgAV, 4D-Fast DIA quantitative proteomics was conducted on renal tissue samples from various groups. Given that the medium dose of ZDZX exhibited therapeutic efficacy comparable to Dex, proteomic analysis was performed on renal tissue samples from the ZDZX-M group. A total of 7450 comparable proteins were identified through the analysis. Figure 6A illustrates a hierarchical clustering heatmap of DEP expression levels across all groups. Comparison between the Model and Sham groups identified 587 DEPs, including 328 up-regulated and 259 down-regulated proteins. Similarly, a comparison of the ZDZX group to the Model group revealed 66 down-regulated and 68 up-regulated proteins in Figure 6B and C. These DEPs encompassed proteins associated with inflammatory pathways (eg, MMP2, IL-17, MPO) and renal function (eg, C3, COL1A1). Notably, the identified DEPs corresponded with several predicted targets from network pharmacology, confirming their involvement in ZDZX's therapeutic effects.

Notably, 27 DEPs were identified as overlapping between the two groups in Figure 6D. Subsequent enrichment analysis indicated that DEPs influenced by ZDZX were predominantly associated with pathways governing peptide hormone secretion and regulation in Figure 6E. KEGG pathway analysis further identified pathways related to the complement and coagulation cascades as well as NET formation in IgAV pathogenesis (Figure 6F). Mechanistically, IgA immune complexes (IgA-ICs) activate neutrophils to release NETs, which in turn trigger complement activation (C3a/C5a). This bidirectional crosstalk establishes a pathogenic feedback loop: complement components enhance neutrophil priming and NETosis, while NET-derived components (eg, histones, cf-DNA) amplify complement activation, exacerbating endothelial damage and vascular leakage.[27,28] These findings collectively suggest that ZDZX exerts therapeutic effects by disrupting this vicious cycle.

Based on the proteomics findings presented, the impact of ZDZX on NET formation in renal tissues was investigated. NETs consist of cf-DNA, myeloperoxidase (MPO), NE, and histones, including citrullinated histone H3 (Cit-H3).[29] It is well established that NET formation is driven by immune-modulatory processes during illness, which subsequently amplify inflammatory cascades.[30] IHC staining revealed pronounced neutrophil infiltration (MPO+) in the renal parenchyma of IgAV model mice, which was markedly reduced by ZDZX treatment in Figure 7C and D. This infiltration was markedly reduced in the ZDZX-treated and Dex groups, indicating decreased neutrophil activation and recruitment.

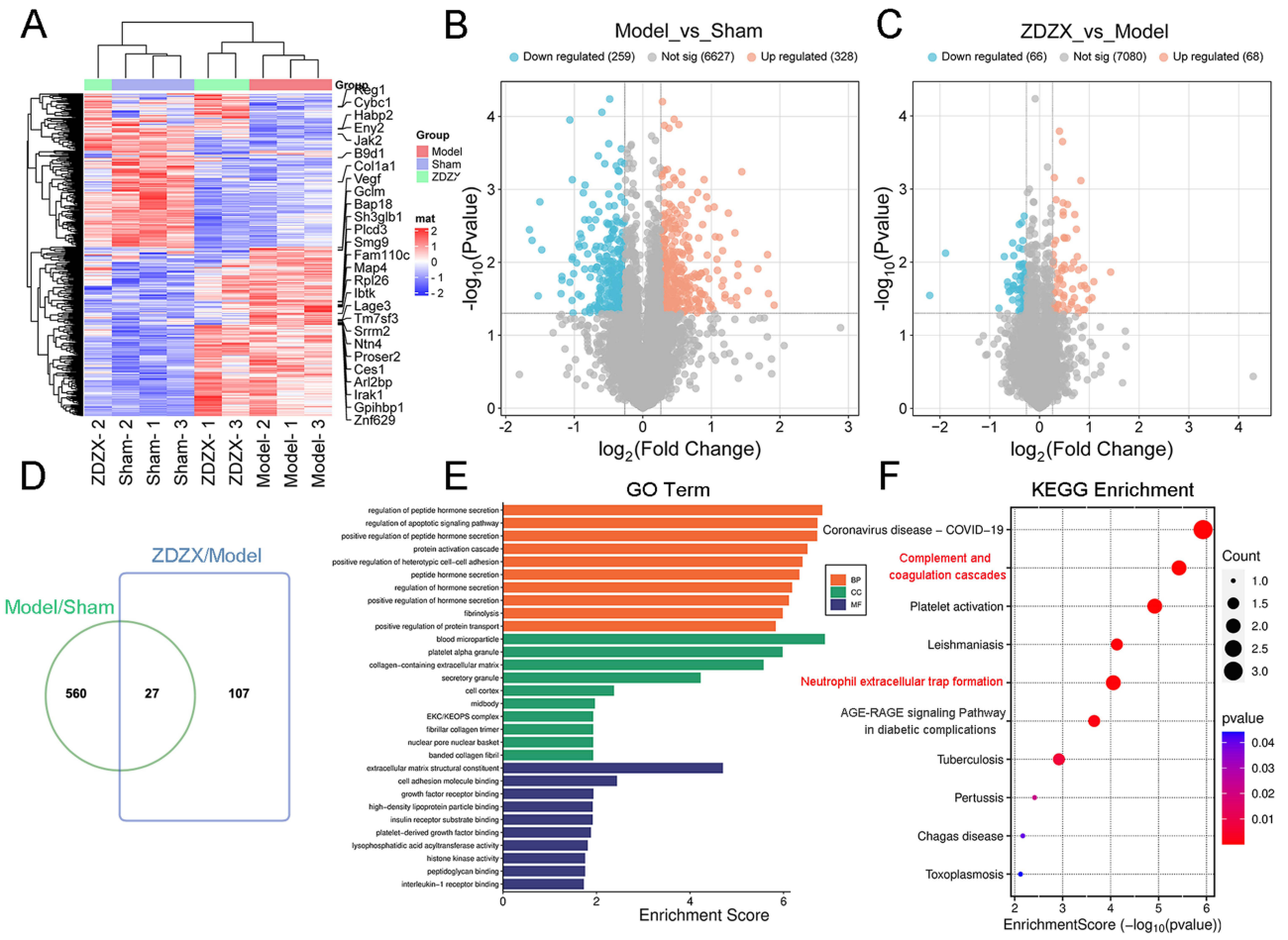

Figure 6 4D-FastDIA Proteomics in kidney. (**A**) The heatmap was constructed to visualize the trends of DEPs in different groups; (**B**) Volcano plot of comparable proteins showing DEPs between model group and sham group, with thresholds of P < 0.05 and |log2 (Fold Change) |≥ 1.2; (**C**) Volcano plot of comparable proteins showing DEPs between ZDZX group and model group, with thresholds of P < 0.05 and log2(Fold Change) > 1.2; (**D**) Venn diagram showing DEPs between model and sham groups, ZDZX and model groups, with enrichment analysis and PPI analysis of overlapping DEPs; (**E**) GO enrichment analysis results of overlapping DEPs; (**F**) KEGG enrichment analysis results of overlapping DEGs; The top 10 KEGG pathways (P < 0.05) were selected. A bubble chart was drawn based on the P-values, with the horizontal axis representing the number of genes enriched in the pathway. The size of the bubble represents the number of genes enriched in the corresponding pathway, and the depth of the color represents significance. Significantly enriched information can be intuitively observed.

Quantitative ELISA confirmed elevated circulating MPO-DNA complexes and Cit-H3 in the model group (P < 0.01), both significantly suppressed by ZDZX (P < 0.05 vs model) in Figure 7. Treatment with medium and high doses of ZDZX, as well as Dex, led to a significant reduction in MPO-DNA and Cit-H3 levels (P < 0.05 or P < 0.01). This aligns with evidence that NETs perpetuate inflammation via complement activation, macrophage pyroptosis, and antigen presentation, suggesting ZDZX mitigates renal injury through NETosis inhibition.

To investigate the impact of ZDZX on the immune system, proinflammatory factors associated with IgAV in mouse kidney tissue were initially examined. As illustrated in Figure 7E–J, ELISA and qRT-PCR analyses revealed elevated levels of proinflammatory cytokines, including IL-6, IL-1β, and IL-17, in the Gliadin-induced IgAV mouse model compared to the sham group. Notably, treatment with ZDZX or Dex significantly decreased the expression of these cytokines, indicating their efficacy in mitigating renal inflammation in Figure 7E–J. In summary, these findings demonstrate that ZDZX treatment inhibits NET formation and suppresses the production of proinflammatory cytokines in the kidney tissue of mice with Gliadin-induced IgAV. This suggests that ZDZX alleviates renal inflammation and prevents tissue damage, highlighting its potential as a therapeutic agent for managing IgAV. Furthermore, the superior therapeutic performance of the ZDZX-M group compared to the dex group emphasizes its efficacy.

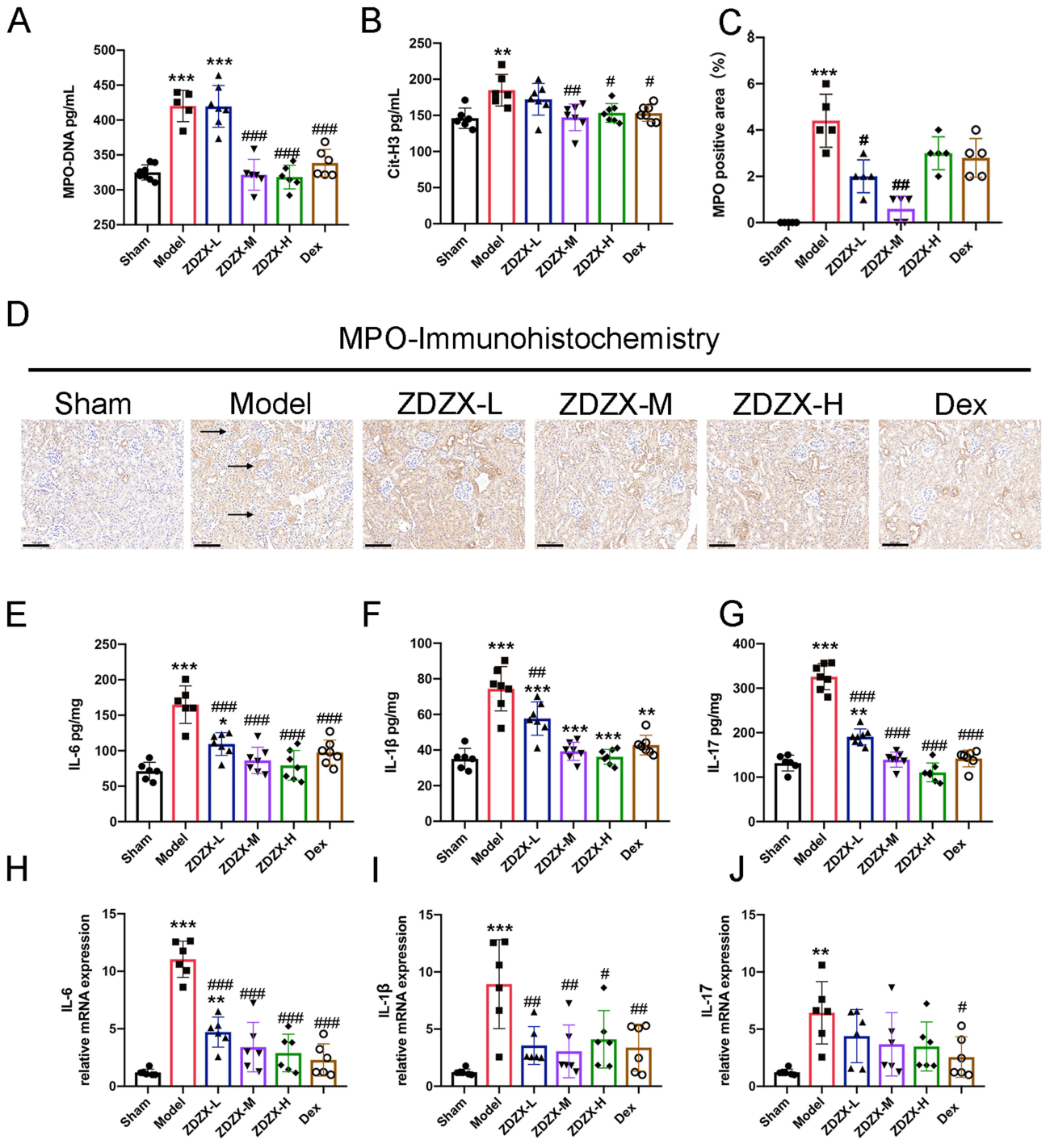

Figure 7 ZDZX reduces hematologic-related indices and inhibits NET formation in the kidney. (**A** and **B**) Serum protein expression level of MPO-DNA and Cit-H3 in kidney tissue from different groups (n=6-8). **P < 0.01, ***P < 0.001 versus the Sham group; #P < 0.05, ##P < 0.01, ####P < 0.001 versus the Model group, respectively. (**C**) MPO activity. Data expressed as mean ± SD (n=3). ***P < 0.001 versus the Sham group; #P < 0.05, ##P < 0.01 versus the Model group, respectively. (**D**) Immunohistochemistry staining of MPO in kidney tissue (n=3). Brown deposits are protein-positive deposits (scale bar: 50 μm). (**E**–**G**) Serum protein expression level of IL-6, IL-1β and IL-17 in kidney tissue from different groups (n=6-8). **P < 0.01, ***P < 0.001 versus the Sham group; ##P < 0.01, ####P < 0.001 versus the Model group, respectively. (**H**–**J**) RT-qPCR expression level of IL-6, IL-1β and IL-17 in kidney tissue from different groups (n=6-8). **P < 0.01, ***P < 0.001 versus the Sham group; #P < 0.05, ##P < 0.01, ####P < 0.001 versus the Model group, respectively.

Discussion

IgAV is a systemic small-vessel vasculitis primarily affecting children and is characterized by non-thrombocytopenic palpable skin purpura, abdominal pain, joint pain, and kidney damage.[31] Although most cases are self-limiting, renal involvement occurs in approximately 40–50% of children and may progress to end-stage renal disease in 1–2%. Current

https://doi.org/10.2147/JIR.S522082

treatment is based on glucocorticoids, but there is still a lack of a uniform regimen for refractory cases.[31,32] For over three decades, ZDZX has been employed in the treatment of IgAV in children, with documented benefits such as reducing disease duration, promoting the healing of skin lesions, and minimizing the risk of renal damage.[13,14] Critically, this study integrates multi-omics and experimental approaches to elucidate ZDZX's novel mechanisms targeting NET-complement crosstalk in IgAV.

The multifaceted nature of TCM is exemplified by the intricate composition and mechanisms of action of ZDZX, which is derived from the renowned traditional formula "Xijiao Dihuang Decoction" and has demonstrated efficacy in treating various infectious diseases.[33] However, the precise underlying mechanisms remain unclear. ZDZX addresses IgAV through a multifaceted approach by utilizing its complex herbal composition to target the disease's intricate pathophysiology. The formula includes herbs with potent anti-inflammatory properties. For example, Lithospermum erythrorhizon has been shown to inhibit the production of proinflammatory cytokines such as TNF-α and IL-6, which are elevated in IgAV patients and contribute to tissue damage.[34] By reducing inflammation, ZDZX alleviates symptoms such as skin purpura, abdominal pain, and joint pain associated with IgAV. Scutellaria baicalensis (Skullcap) is abundant in flavonoids like baicalin, which have been reported to suppress the activation of inflammatory pathways, including the NF-κB pathway.[35] This inhibition reduces inflammation and protects tissues from damage caused by IgAV. Paeonia lactiflora contains paeoniflorin, which has been demonstrated to reduce proteinuria in IgAV patients.[35] This herb preserves renal function by stabilizing the glomerular filtration barrier and preventing protein leakage into the urine.

Previous studies have established IgAV models in rats and rabbits through the administration of Chinese herbs, followed by OVA and Freund's complete buffer.[36] In the present study, gliadin was employed as a dietary antigen to continuously stimulate the mucosal immune system, leading to immune complex formation following the impairment of the reticuloendothelial system with Indian ink. This approach closely simulates the pathogenesis of IgAV, providing a reliable model for assessing the efficacy and mechanism of action of ZDZX.[25] The findings of this study demonstrate that ZDZX significantly mitigates renal inflammation and enhances renal function in a mouse model of IgAV. These results emphasize the therapeutic potential of ZDZX in addressing renal complications associated with IgAV. Clinically, patients with IgAV exhibit significantly elevated levels of blood urea nitrogen (BUN) and creatinine compared to healthy individuals.[37] The results of this study indicate that ZDZX significantly reduced serum BUN and creatinine levels in IgAV mice, suggesting an improvement in renal function. This effect was comparable to that of Dex, a corticosteroid known for its anti-inflammatory properties. The renal protective effect of ZDZX was further corroborated by histomorphological assessments, which revealed reductions in renal interstitial collagen deposition and glomerular basement membrane thickness, resembling findings observed in kidney biopsies from IgAV patients.[38] In clinical practice, IgAVN is a common complication of IgA vasculitis and represents the most frequent secondary glomerulopathy in pediatric populations.[39] These findings suggest that the timely administration of ZDZX treatment may effectively mitigate renal pathological damage and provide substantial benefits in preserving kidney function in patients with IgAV.

Previous investigations have suggested that the progression of renal damage in IgAN may be exacerbated by proinflammatory cytokines, including IL-6, IL-1β, and TNF-α.[40] The involvement of IL-1β in IgAV pathogenesis, as evidenced by its role in neutrophil activation and Th17 cell differentiation, aligns with the intricate inflammatory dynamics characteristic of autoimmune diseases.[41] Serum levels of IL-17 and IL-6 may serve as clinical biomarkers for the nonsurgical assessment of kidney damage in IgAN patients, reflecting the extent of renal injury.[42,43] ZDZX appears to exert its therapeutic effects through the inhibition of neutrophil activation, suppression of proinflammatory cytokine release, and modulation of the complement system. This multifaceted approach results in reduced renal inflammation and tissue damage, as demonstrated by decreased levels of MPO-DNA, Cit-H3, and proinflammatory cytokines, including IL-6, IL-1β, and IL-17. Furthermore, ZDZX treatment was observed to reduce IgA deposition in renal tissue, potentially by downregulating inflammatory cytokine expression. This finding is noteworthy, as it highlights a potential mechanism by which ZDZX confers renal protection against IgAV-associated injury.

This study highlights the role of NETs in IgAV. NETs, which consist of DNA, histones, and antimicrobial proteins, have been implicated in various autoimmune diseases due to their involvement in promoting inflammation and tissue damage.[44] Recent advances in NET-complement crosstalk have highlighted the critical role of neutrophil extracellular traps (NETs) in amplifying vascular inflammation and renal injury in pediatric IgAV. Elevated NETosis levels in IgAV

patients correlate with disease activity and renal dysfunction, NETs promote vascular damage through IgA immune complex deposition and complement activation.[45] We reinforce the value of our NET-complement findings by citing emerging evidence that NETs are central to IgAV pathogenesis. Although the findings of this study provide valuable insights into the potential mechanisms of ZDZX in IgAV, further investigation is required to delineate its precise molecular mechanisms. While animal models provide important mechanistic insights, they inherently limit direct translation to human pathophysiology. To bridge this gap and enhance translational relevance, we propose human-based approaches in future research, such as organ-on-chip systems incorporating patient-derived endothelial cells and immune components, or mechanistic studies using patient-derived neutrophils. Future research should also aim to elucidate the multi-system and multi-target therapeutic efficacy of ZDZX's active components and identify optimal therapeutic dosages. Long-term clinical studies are essential to comprehensively evaluate ZDZX's therapeutic potential in IgAV.

In summary, the therapeutic potential of ZDZX in mitigating renal inflammation and enhancing renal function in IgAV is emphasized by these findings. Its capacity to modulate NET formation and exert anti-inflammatory effects highlights its promise as a novel therapeutic agent. Future investigations should focus on further elucidating its mechanisms of action and optimizing its clinical application.

Conclusion

The findings of this study demonstrate that ZDZX significantly mitigates renal inflammation and enhances renal function in a mouse model of IgAV. These results highlight the therapeutic potential of ZDZX in addressing renal complications associated with IgAV, suggesting its potential as a viable treatment option. Importantly, these experimental findings align with the long-standing clinical application of ZDZX for over 30 years at the Affiliated Hospital of Changchun University of Chinese Medicine, where its safety and efficacy in treating pediatric IgAV are well-documented. The therapeutic effects of ZDZX are achieved through the inhibition of neutrophil activation, the reduction of proinflammatory cytokines, and the modulation of NET formation. Future investigations should prioritize dose-optimized clinical trials to determine the optimal therapeutic window for human patients, alongside mechanistic studies to validate biomarkers of treatment response.

Abbreviations

ZDZX, Zidian Zhenxiao granule; TCM, Traditional Chinese Medicine; HSP, Henoch-Schonlein purpura; KEGG, Kyoto Encyclopedia of Genes and Genomes; GO, gene ontology; IL, Interleukin; H&E, Hematoxylin and eosin; Masson, Masson's trichrome stain; PAS, Periodic Acid-Schiff stain; IgAV, immunoglobulin A vasculitis; MPO-DNA, myeloperoxidase-DNA; ELISA, enzyme linked immunosorbent assay; NETs, Neutrophil Extracellular Traps; IHC, Immunohistochemistry; IF, immunofluorescence; MMF, Mycophenolate mofetil; IVIG, Intravenous Immunoglobulin; OB, oral bioavailability; DL, drug-likeness; DAVID, Database for Annotation, Visualization, and Integrated Discovery; BUN, blood urea nitrogen; WBC, white blood cell; LYMPH, lymphocyte; PLT, platelet; BUN, blood urea nitrogen; DEP, differentially expressed proteins.

Acknowledgments

The authors greatly appreciate the editors and peer reviewers for their critical readings and insightful comments, which were helpful in substantially improving the paper.

Author Contributions

All authors made a significant contribution to the work reported, whether that is in the conception, study design, execution, acquisition of data, analysis, and interpretation, or in all these areas; took part in drafting, revising, or critically reviewing the article; gave final approval of the version to be published; have agreed on the journal to which the article has been submitted; and agree to be accountable for all aspects of the work.

Funding

This work was funded by grants from the Science and Technology Development Plan of Jilin Province (No. YDZJ202201ZYTS202).

Disclosure

The authors affirm that this research was performed without any commercial or financial associations that might be interpreted as potential conflicts of interest.

References

1. Martina H, Ana K, Mario S, et al. Insight into the Interplay of Gd-IgA1, HMGB1, RAGE and PCDH1 in IgA Vasculitis (IgAV). *Int J Mol Sci*. 2024;25(8). doi:10.3390/ijms25084383
2. Xu L, Li Y, Wu X. IgA vasculitis update: epidemiology, pathogenesis, and biomarkers. *Front Immunol*. 2022;13:921864. doi:10.3389/fimmu.2022.921864
3. Gardner-Medwin J, Dolezalova P, Cummins C, Southwood T. Incidence of Henoch-Schönlein purpura, Kawasaki disease, and rare vasculitides in children of different ethnic origins. *Lancet*. 2002;360(9341):1197–1202. doi:10.1016/s0140-6736(02)11279-7
4. Xianxian J, Hua Z, Qinglian J, et al. Identification of key genes and imbalance of immune cell infiltration in immunoglobulin A associated vasculitis nephritis by integrated bioinformatic analysis. *Front Immunol*. 2023;14. doi:10.3389/fimmu.2023.1087293
5. Xu S, Han S, Dai Y, Wang L, Zhang X, Ding Y. A review of the mechanism of vascular endothelial injury in immunoglobulin a vasculitis. *Front Physiol*. 2022;13:833954. doi:10.3389/fphys.2022.833954
6. Xiu-Qi C, Li T, Qing T, Li H, Yuan-Han Q. An emerging role for neutrophil extracellular traps in IgA vasculitis: a mini-review. *Front Immunol*. 2022;13. doi:10.3389/fimmu.2022.912929
7. Xiu-Qi C, Li T, Jia-Sen Z, Shi-Qun Z, Yan-Jun Z, Yuan-Han Q. The involvement of neutrophil extracellular traps in disease activity associated with IgA vasculitis. *Front Immunol*. 2021;12. doi:10.3389/fimmu.2021.668974
8. Skendros P, Mitsios A, Chrysanthopoulou A, et al. Complement and tissue factor-enriched neutrophil extracellular traps are key drivers in COVID-19 immunothrombosis. *J Clin Invest*. 2020;130(11):6151–6157. doi:10.1172/jci141374
9. Colón DF, Wanderley CW, Franchin M, et al. Neutrophil extracellular traps (NETs) exacerbate severity of infant sepsis. *Crit Care*. 2019;23(1):113. doi:10.1186/s13054-019-2407-8
10. Xuerong Y, Qi L, Yuanyuan H, et al. Individualized medication based on pharmacogenomics and treatment progress in children with IgAV nephritis. *Front Pharmacol*. 2022;13. doi:10.3389/fphar.2022.956397
11. Ozen S, Marks S, Brogan P, et al. European consensus-based recommendations for diagnosis and treatment of immunoglobulin A vasculitis-the SHARE initiative. *Rheumatology*. 2019;58(9):1607–1616. doi:10.1093/rheumatology/kez041
12. Okano M, Fujieda S, Gotoh M, et al. Executive summary: Japanese guidelines for allergic rhinitis 2020. *Allergol Int*. 2023;72(1):41–53. doi:10.1016/j.alit.2022.11.003
13. Lu L. Clinical observation on the treatment of Henoch-Schonlein Purpura (Wind-heat Shangluo Syndrome) with Xiaoer Purpura Zhixiao Granule. *Master*. 2022;100(51):e28291. doi:10.26980/d.cnki.gcczc.2022.000291
14. Cui Q, Wang Z, Zhu H, Feng X. Analysis of chemical constituents of Xiaoer Purpura Zexiao granules based on UPLC-Q-Orbitrap-MS. *Chin J Trad Chin Med*. 2020;35(05):2558–2562.
15. Guo G, Liu Z, Yu J, et al. Neutrophil function conversion driven by immune switchpoint regulator against diabetes-related biofilm infections. *Adv Mater*. 2024;36(8):e2310320. doi:10.1002/adma.202310320
16. Liu Z, Qin X, Nong K, et al. Oral administration of LfcinB alleviates DSS-induced colitis by improving the intestinal barrier and microbiota. *Food Funct*. 2024;15(4):2038–2051. doi:10.1039/d3fo05236b
17. Jiang Q, Chi X, Wei T, et al. Amelioration of immunoglobulin A vasculitis by suppression of the pathological expansion of T follicular helper 17 cells. *J Autoimmun*. 2024;149:103304. doi:10.1016/j.jaut.2024.103304
18. Li X, Liu Z, Liao J, Chen Q, Lu X, Fan X. Network pharmacology approaches for research of Traditional Chinese Medicines. *Chinese J Nat Med*. 2023;21(5):323–332. doi:10.1016/s1875-5364(23)60429-7
19. Monti C, Zilocchi M, Colugnat I, Alberio T. Proteomics turns functional. *J Proteomics*. 2019;198:36–44. doi:10.1016/j.jprot.2018.12.012
20. Xin W, Zi-Yi W, Jia-Hui Z, Shao L. TCM network pharmacology: a new trend towards combining computational, experimental and clinical approaches. *Chin J Nat Med*. 2021;19(1). doi:10.1016/s1875-5364(21)60001-8
21. Paolacci S, Precone V, Acquaviva F, et al. Genetics of lipedema: new perspectives on genetic research and molecular diagnoses. *Eur Rev Med Pharmacol Sci*. 2019;23(13). doi:10.26355/eurrev_201907_18292
22. Allan Peter D, Cynthia JG, Robin JJ, et al. The comparative toxicogenomics database: update 2017. *Nucleic Acids Res*. 2016;45. doi:10.1093/nar/gkw838
23. Joanna SA, Carol AB, François S, Alan FS, Ada H. OMIM.org: online Mendelian Inheritance in Man (OMIM®), an online catalog of human genes and genetic disorders. *Nucleic Acids Res*. 2014;43. doi:10.1093/nar/gku1205
24. Philippe B, Jérôme M, Frédéric E, Christophe D, Christophe K. jvenn: an interactive Venn diagram viewer. *BMC Bioinf*. 2014;15(1). doi:10.1186/1471-2105-15-293
25. Chen XQ, Zou JS, Tu L, Yun X, Qin YH. Neutrophil extracellular traps involved in the pathogenesis of IgA vasculitis: confirmed in two IgAV rat models. *PLoS One*. 2023;18(7):e0288538. doi:10.1371/journal.pone.0288538
26. Wanfa D, Dan L, Tingting Z, Qi Y, Fengjie H, Jie W. Oral delivery of staphylococcal nuclease ameliorates DSS induced ulcerative colitis in mice via degrading intestinal neutrophil extracellular traps. *Ecotoxicol Environ Saf*. 2021;215. doi:10.1016/j.ecoenv.2021.112161
27. Leffler J, Martin M, Gullstrand B, et al. Neutrophil extracellular traps that are not degraded in systemic lupus erythematosus activate complement exacerbating the disease. *J Immunol*. 2012;188(7):3522–3531. doi:10.4049/jimmunol.1102404

28. Burmeister A, Vidal-Y-Sy S, Liu X, et al. Impact of neutrophil extracellular traps on fluid properties, blood flow and complement activation. *Front Immunol*. 2022;13:1078891. doi:10.3389/fimmu.2022.1078891
29. Ludwig TW, Ulrich G, Andreas U, et al. Midkine drives cardiac inflammation by promoting neutrophil trafficking and NETosis in myocarditis. *J Exp Med*. 2019;216(2). doi:10.1084/jem.20181102
30. Venizelos P. Neutrophil extracellular traps in immunity and disease. *Nat Rev Immunol*. 2017;18(2). doi:10.1038/nri.2017.105
31. Maria Goretti Moreira Guimarães P, Lilian Monteiro Pereira P. IgA vasculitis in children. *J Bras Nefrol*. 2022;44(1). doi:10.1590/2175-8239-jbn-2022-e002
32. Louise O, Sunil S. Childhood IgA Vasculitis (Henoch Schonlein Purpura)-advances and knowledge gaps. *Front Pediatr*. 2019;7. doi:10.3389/fped.2019.00257
33. Lu J, Yan J, Yan J, et al. Network pharmacology based research into the effect and mechanism of Xijiao Dihuang decoction against sepsis. *Biomed Pharmacothe*. 2020;122:109777. doi:10.1016/j.biopha.2019.109777
34. Song Y, Huang X, Yu G, et al. Pathogenesis of IgA vasculitis: an up-to-date review. *Front Immunol*. 2021;12:771619. doi:10.3389/fimmu.2021.771619
35. Ma S, Zhao M, Chang M, Shi X, Shi Y, Zhang Y. Effects and mechanisms of Chinese herbal medicine on IgA nephropathy. *Phytomedicine*. 2023;117:154913. doi:10.1016/j.phymed.2023.154913
36. Yanhong L, Xiaochun F, Lan H, et al. Hematologic and immunological characteristics of Henoch-Schönlein purpura in rat and rabbit models induced with ovalbumin based on type III hypersensitivity. *Sci Rep*. 2015;5. doi:10.1038/srep08862
37. Alojzija H, Ziga R, Vesna J, et al. IgA vasculitis in adults: the performance of the EULAR/PRINTO/PRES classification criteria in adults. *Arthritis Res Ther*. 2015;18. doi:10.1186/s13075-016-0959-4
38. Julian F, Maren B, David K, Stefan P, Raoul B. Clinical and histological comparison of IgA nephritis and renal IgA vasculitis. *Nephrol Dial Transplant*. 2024. doi:10.1093/ndt/gfae143
39. Alexander KCL, Benjamin B, Kin Fon L. Henoch-Schönlein Purpura in children: an updated review. *Curr Pediatr Rev*. 2020;16(4). doi:10.2174/1573396316666200508104708
40. Lu Y, Yan W, Aobulikasimu N, et al. Effects of periostracum cicadae on cytokines and apoptosis regulatory proteins in an IgA nephropathy rat model. *Int J Mol Sci*. 2018;19(6). doi:10.3390/ijms19061599
41. Charles AD. A clinical perspective of IL-1β as the gatekeeper of inflammation. *Eur J Immunol*. 2011;41(5). doi:10.1002/eji.201141550
42. Wenjun Z, Shi F, Yucheng W, et al. Elevated urinary IL-6 predicts the progression of IgA nephropathy. *Kidney Int Rep*. 2023;8(3). doi:10.1016/j.ekir.2022.12.023
43. Christian FK, Tilman S, Jan-Hendrik R, Ulf P. T helper type 17 cells in immune-mediated glomerular disease. *Nat Rev Nephrol*. 2017;13(10). doi:10.1038/nrneph.2017.112
44. Groza Y, Jemelkova J, Kafkova LR, Maly P, Raska M. IL-6 and its role in IgA nephropathy development. *Cytokine Growth Factor Rev*. 2022;66:1–14. doi:10.1016/j.cytogfr.2022.04.001
45. Zhang Y, Xu G. IgA vasculitis with nephritis: an overview of the pathogenesis and clinical characteristics. *Clin Exp Rheumatol*. 2025;43(4):728–741. doi:10.55563/clinexprheumatol/mjhyff